Int. J. Electrochem. Sci., 9 **(2014)** 1232 - 1249

International Journal of
ELECTROCHEMICAL
SCIENCE
www.electrochemsci.org

Multiple Redox-Active Sites in Copper Dipyrromethene−Corrole Self-Assembled Monolayers Deposited onto Gold Electrodes

Iwona Grabowska[1], *Wouter Maes*[2,3], *Thien Huynh Ngo*[2,4], *Taoufik Rohand*[2], *Wim Dehaen*[2], *Jerzy Radecki*[2,#], *Hanna Radecka*[1,#,*]

[1]Institute of Animal Reproduction and Food Research of the Polish Academy of Sciences, Tuwima 10, 10-748 Olsztyn, Poland
[2]KU Leuven, Chemistry Department, Celestijnenlaan 200F, B-3001 Leuven, Belgium
[3]Design & Synthesis of Organic Semiconductors (DSOS), Institute for Materials Research (IMO-IMOMEC Ass. Lab.), Hasselt University, Universitaire Campus, Agoralaan 1 - Building D, B-3590 Diepenbeek, Belgium
[4] ICYS-Researcher, International Center for Young Scientists (ICYS), International Center for Materials Nanoarchitectonics (MANA), National Institute for Materials Science (NIMS), Namiki 1-1, Tsukuba, Ibaraki 305-0044, Japan
[#] ISE Member
[*]E-mail: h.radecka@pan.olsztyn.pl

Received: 30 October 2013 / *Accepted:* 21 November 2013 / *Published:* 5 January 2014

In this work, both separate dipyrromethene and copper corrole derivatives and a specifically designed copper corrole-dipyrromethene conjugate were applied for gold electrode modification. The various oligopyrrole materials were used for copper complexation toward the preparation of different types of electroactive self-assembling monolayers (SAMs): (i) a copper dipyrromethene (**Cu-DPM**) SAM, (ii) a copper corrole (**Cu-COR**) SAM, and (iii) a copper dipyrromethene-copper corrole conjugate (**Cu-DPM-Cu-COR**) SAM. The SAMs incorporating the single Cu sites as well as, two Cu sites located in one molecule, one over another, were characterized by cyclic voltammetry, Osteryoung square-wave voltammetry and electrochemical impedance spectroscopy.

Keywords: dipyrromethene, corrole, self-assembled monolayers, copper complexation, mono- and multi-redox sites

1. INTRODUCTION

In recent years there is a growing interest in the creation of multilayer surface architectures containing metal complexes starting from molecular building blocks [1,2]. Many molecules have been

designed and synthesized to obtain redox- and photofunctional molecular wires at the surface, which could find application in the development of photo- and electrochemical sensors, and biosensors [2]. Some very recent examples include methods for assembling multilayers of metallo-terpyridine on a gold surface [2,3,4], self-assembled peptide nanofibrils used as biorecognition elements for the complexation with copper ions [5], or layer-by-layer assembly of viologenthiol-functionalized carbon nanotubes via coordination with Cu(II) ions [6]. These systems were electrochemically characterized, but in most cases in organic solvents only. Redox-active polypyridyl complexes sequentially assembled on gold electrodes have also been reported [7-9]. An overview of the state-of-the-art of surface modifications using terpyridine systems was recently provided by Schubert and co-workers [10] and Nishihara et al. [2]. The thiol-modified terpyridine ligand and its complexes with Co, Cr, and Os were described by Abruna and Markus [7]. These authors have demonstrated the preparation of redox-active mono- and multimetallic systems capable of sequential self-assembly onto gold surfaces, and they performed an electrochemical characterization in aqueous solutions.

Within our groups, porphyrinoid chemistry has been an ongoing joint research topic [11-20]. The synthesis, metallation/demetallation protocols, photophysical properties and functionalization of *meso*-pyrimidinylcorroles have caught our particular attention in recent years [14-19]. Corroles are porphyrin analogues lacking one *meso*-carbon atom and these contracted porphyrinoids display some peculiar properties distinct from their porphyrin congeners. Cu-metallated corroles are of interest to many scientists active in the field as they exhibit an interesting electronic configuration with a hybrid Cu(III)-Cu(II) π-cation character [21]. In previous collaborative work, we have reported the determination of the surface acidity of a free-base corrole in a self-assembled monolayer (SAM) [20]. The research presented here is the result of our continued joint interest in redox-active SAMs [22] and is inspired by previous work in which electroactive monolayers were prepared based on complexation of Cu(II) on a gold surface modified with SAMs containing a dipyrromethene derivative [23,24].

The chelates of the transition metals Cu(II), Ni(II) and Zn(II) with dipyrromethene compounds have been reported some time ago [25-27]. However, electrochemical characterization of such complexes was until now only carried out in organic solvents [28]. The kinetics of electron transfer in the tetrahedrally coordinated copper(II)/copper(I) couple was described on a Pt electrode using AC voltammetry in acetone [28], in which the complex Cu^{II}-dipyrromethene ($Cu^{II}(dpym)_2^0$) (dpym = 3,3',5,5'-tetramethyl-4.4'-dicarboethoxydipyrro-methene) was reduced to the four-coordinated anion $Cu^{I}(dpym)_2^-$. The electrochemistry of metallocorroles is also of great interest, mainly due to the ability of the trianionic corrole ligand to stabilize high-valent transition metal centers [21,29-31].

In this work we present the immobilization of redox-active single copper corrole and dipyrromethene complexes and a copper corrole-dipyrromethene conjugate onto gold electrodes and subsequent electrochemical characterization of their redox activity on the surface. The characterization of the SAMs was done by cyclic voltammetry (CV), Osteryoung square-wave voltammetry (OSWV), electrochemical impedance spectroscopy (EIS).

To the best of our knowledge, this is the first work in which electrochemical characterization of a copper corrole and a novel copper corrole-copper dipyrromethene conjugate (with multiple redox-active sites) self-assembled on gold electrodes is carried out in aqueous solutions.

2. MATERIALS AND METHODS

2.1. Chemicals

N-(3-Dimethylaminopropyl)-*N'*-ethylcarbodiimide hydrochloride (EDC), 2-aminoethanethiol hydrochloride 98% (AET), 11-mercaptopropionic acid, and copper(II) acetate were obtained from Fluka-Sigma-Aldrich (Poznań, Poland). Ethanol, methanol, chloroform, potassium nitrate, potassium chloride, ammonia, and trifluoroacetic acid were obtained from POCh (Gliwice, Poland). All aqueous solutions were prepared with deionized and charcoal-treated water (resistivity of 18.2 MΩ cm), purified with a Milli-Q reagent grade water system (Millipore, Bedford, MA).

2.2. Synthesis

The synthesis of the carboxyphenyl-substituted dipyrromethene derivative (5-(4-carboxyphenyl)-4,6-dipyrrin, DPM-COOH) has been disclosed before [19]. The 4-aminophenyl-substituted copper corrole (Cu-10-(4-aminophenyl)-5,15-dimesitylcorrole, Cu-COR-NH_2) was synthesized according to a recently published procedure [32]. The copper corrole-dipyrromethene conjugate (Cu-COR-DPM) was synthesized in three steps, as outlined in Scheme 1.

10-(4-Formylphenyl)-5,15-bis(2,4,6-trimethylphenyl)corrolato copper. Cu-10-(4-cyano-phenyl)-5,15-dimesitylcorrole [17] (205 mg, 0.29 mmol) was dissolved in toluene (5 mL) and the solution was cooled down to 0 °C. DIBAL-H (1 mL of a 1.08 M solution in hexane) was added drop wise under N_2 and the resulting mixture was stirred for 1 h at 0 °C. $CHCl_3$ (5 mL) and a 10% HCl solution (5 mL) were subsequently added and the mixture was stirred for 1 h at rt. CH_2Cl_2 (50 mL) was added and the mixture was washed with water (3 × 25 mL), dried over $MgSO_4$, filtered and the solvent was removed under reduced pressure. After flash column chromatography (silica, eluent CH_2Cl_2), pure Cu-10-(4-formylphenyl)-5,15-dimesitylcorrole was obtained as a red-brown solid (172 mg, 85%). MS (ESI+) *m/z* 700.7 $[M+H]^+$; ^{1}H NMR (300 MHz, CDCl3) δ 10.12 (s, 1H; CHO), 8.02−7.96 (m, 4H; H_{Ph} + H_β), 7.77 (d, ^3J = 4.1 Hz, 2H; H_β), 7.37 (s_{br}, 2H; H_β), 7.18 (s_{br}, 2H; H_β), 7.08−7.01 (m, 6H; H_{Ph} + H_{mesit}), 2.40 (s, 6H; CH_3), 2.06 (s, 12H; CH_3); ^{13}C NMR (75 MHz, CDCl3) δ 192.1 (CHO), 148.9, 144.5, 143.9, 137.8, 136.3, 132.8, 131.7, 131.2, 129.6 (CH), 128.6 (CH), 128.3, 128.0, 121.5, 21.3 (CH_3), 19.9 (CH_3).

10-(4-Dipyrromethylphenyl)-5,15-bis(2,4,6-trimethylphenyl)corrolato copper. Cu-10-(4-formylphenyl)-5,15-dimesitylcorrole (78.7 mg, 0.118 mmol) was stirred in 20 mL of pyrrole under nitrogen atmosphere. HCl (0.5 mL) was added and after 30 min the excess of pyrrole was evaporated under reduced pressure. Flash column chromatography (silica, eluent gradient from pure petroleum ether to pure dichloromethane) afforded the pure copper corrole-dipyrromethane conjugate (32.1 mg, 35%). MS (ESI+): calcd for $C_{52}H_{43}CuN_6$: 814.3; found: *m/z* 815.7 $[M+H]^+$; ^{1}H NMR (300 MHz, $CDCl_3$, 25°C, TMS): δ 7.99−7.95 (m, 4H, H_{NH}+H_β), 7.54 (d, J = 7.3, 2H, H_{Ph}), 7.34−7.31 (m, 4H, H_β), 7.23 (s, 4H, H_{Ph}), 7.01 (s, 4H, H_{Ph}), 6.72 (s, 2H, H_β), 6.18 (s_{br}, 2H, H_β), 5.96 (s, 2H, H_β), 5.56 (s, 1H), 2.39 (s, 6H), 2.05 (s, 12H); ^{13}C NMR (75 MHz, $CDCl_3$) δ 148.8, 144.2, 143.6, 142.5, 137.5, 132.2,

130.9 (CH), 128.1/128.0 (CH), 121.1 (CH), 117.5 (CH), 108.5 (CH), 107.4 (CH), 21.2 (CH_3), 19.8 (CH_3).

10-(4-Dipyrromethenylphenyl)-5,15-bis(2,4,6-trimethylphenyl)corrolato copper. A solution of copper 10-(4-dipyrromethylphenyl)-5,15-dimesitylcorrole (32 mg, 0.039 mmol) and *p*-chloranil (29 mg, 0.118 mmol) in dichloromethane (100 mL) was stirred at reflux temperature under nitrogen atmosphere for 2 h. After purification by flash column chromatography (silica, eluent CH_2Cl_2), the corrole-dipyrromethene conjugate (27.6 mg, 86%) was obtained. MS (ESI+): calcd for $C_{52}H_{41}CuN_6$: 812.3; found: *m/z* 813.7 $[M+H]^+$; ^1H NMR (300 MHz, $CDCl_3$, 25°C, TMS): δ 7.88 (s_{br}, 2H, H_β), 7.59−7.54 (m, 6H, $H_{Ph}+H_\beta$), 7.29 (s_{br}, 2H, H_β), 7.16−7.15 (m, 4H, $H_{Ph}+H_\beta$), 6.94 (s, 4H, H_{Ph}), 6.65 (d, J = 3.6, 2H, H_β), 6.36 (d, J = 3.6, 2H, H_β), 2.32 (s, 6H), 1.99 (s, 12H); ^{13}C NMR (75 MHz, $CDCl_3$) δ 148.8, 143.8 (CH), 141.5, 140.6, 137.6/137.5, 131.2 (CH), 130.6 (CH), 128.9 (CH), 128.1 (CH), 121.2 (CH), 117.7 (CH), 21.2 (CH_3), 19.8 (CH_3).

2.3. Modification of the electrodes

Two types of electrodes were used for the experiments:

- Gold disk electrodes, 2 mm^2 area (Bioanalytical Systems (BAS), West Lafayette, IN)
- Gold substrates: 1cm x 1cm of mica covered by 10 nm Ti and 100 nm Au (IMEC, Leuven, Belgium)

The gold disk electrodes were polished with wet 0.3 and 0.05 μm alumina slurry (Alpha and Gamma Micropolish; Buehler, Lake Bluff, IL) on a flat pad for at least 10 min and rinsed repeatedly with water and finally cleaned in a sonicator (1 min). The polished electrodes were then dipped in 0.5 M KOH solution, deoxygenated by purging with argon for 15 min, and the potential was cycled between -400 and -1200 mV (versus an Ag/AgCl reference electrode) with a scan rate of 100 mVs^{-1} until the cyclic voltammograms showed no further changes. The gold substrates were washed with acetone and subsequently with ethanol, followed by annealing in a hydrogen flame three times during 2 min.

Surface modification using DPM-COOH (Scheme 2, Cu-DPM SAM). After cleaning, the gold surface of the electrodes was immediately immersed into a 0.1 M solution of AET in ethanol for 3 h. Then, the electrodes were modified with a solution of 0.001 M DPM-COOH and 0.26 M EDC in chloroform and methanol (volume ratio 1:1) for 18 h. Next, they were exposed to a 0.001 M solution of copper(II) acetate in chloroform and methanol (1:1 volume ratio) for 12 h. Subsequently, the electrodes were again dipped into a 0.001 M solution of DPM-COOH in chloroform and methanol (volume ratio 1:1) for 18 h.

Surface modification using Cu-COR (Scheme 2, Cu-COR SAM). In this case, the gold electrodes were, immediately after cleaning, put into a 0.001 M solution of mercaptopropionic acid in ethanol (with addition of 2 v% trifluoroacetic acid) for 18 h. Then, the electrodes were rinsed with 10% (v/v) ammonia in ethanol and the COOH groups were activated for amide coupling by a 0.26 M solution of EDC in chloroform and methanol (volume ratio 1:1) for 18 h. Next, the electrodes were dipped in a 0.001 M solution of Cu-COR-NH_2 in ethanol for 24 h.

Surface modification using Cu-COR-DPM (Scheme 2, Cu-DPM-Cu-COR SAM). For this modification, the gold surface of the electrodes was immediately immersed into a 0.1 M solution of AET in ethanol for 3 h. Then, the electrodes were modified with a 0.001 M DPM-COOH solution and a 0.26 M EDC solution in chloroform and methanol (volume ratio 1:1) for 18 h. Next, they were exposed to a 0.001 M solution of copper(II) acetate in chloroform and methanol (volume ratio 1:1) for 12 h. In the last step, the electrodes were immersed in a 0.001 M ethanol solution of Cu-COR-DPM for 18 h.

The solutions used for modification were put into 8 mm diameter tubes (no flat bottom). After dipping the electrodes, the tubes were sealed with Teflon tape to prevent solvent evaporation. After modification, the electrodes were rinsed with ethanol or chloroform from the modification solution. All modified gold electrodes were stored at 4 ºC in a 0.1 M KCl solution until use.

2.4. Electrochemical measurements

All electrochemical measurements were performed with a potentiostat–galvanostat AutoLab (Eco Chemie, Utrecht, The Netherlands) with a three electrode configuration. Potentials were measured *versus* the Ag/AgCl electrode, and a platinum wire was used as the auxiliary electrode. Cyclic voltammetry (CV) was performed in 0.1 M KCl solution and the potential was cycled:

- for Cu-DPM SAM: from 600 mV to -200 mV and back
- for Cu-COR SAM: from 700 mV to -900 mV and back
- for Cu-DPM-Cu-COR SAM: from 600 mV to – 700 mV for, with a scan rate of 100 mVs^{-1} , until the CV showed no further changes (about 10 scans).

Osteryoung square-wave voltammetry was performed using the following parameters: step potential 10 mV, square-wave frequency 25 Hz, and square-wave amplitude 25 mV. Electrochemical impedance spectroscopy measurements were performed within the frequency range of 0.1 to 10 kHz, with ac amplitude of 10 mV in a solution containing 0.1 M KCl in the presence of $K_3[Fe(CN)_6]/K_4[Fe(CN)_6]$ (0.5 mM each), at the formal potential of the redox couple (170 mV). Electrochemical impedance spectroscopy measurements performed in 0.1 M KCl in the absence of an external redox probe were recorded at the approximate formal potential of the redox-active molecules [33,34]: ~ + 230 mV for the Cu-DPM SAM, ~ - 240 mV for the Cu-COR SAM, and at ~ + 180 mV and ~ - 260 mV for the Cu-DPM-Cu-COR SAM.

3. RESULTS AND DISCUSSIONS

For this study, a novel copper corrole-dipyrromethene conjugate Cu-COR-DPM was specifically designed and synthesized. The synthetic protocol started from the easily available *meso*-4-cyanophenyl-substituted copper corrole [17], which was converted to the 4-formylphenyl derivative by treatment with DIBAL-H. Further built-up of the dipyrromethene from the formyl group was performed by standard reactions (Scheme 1).

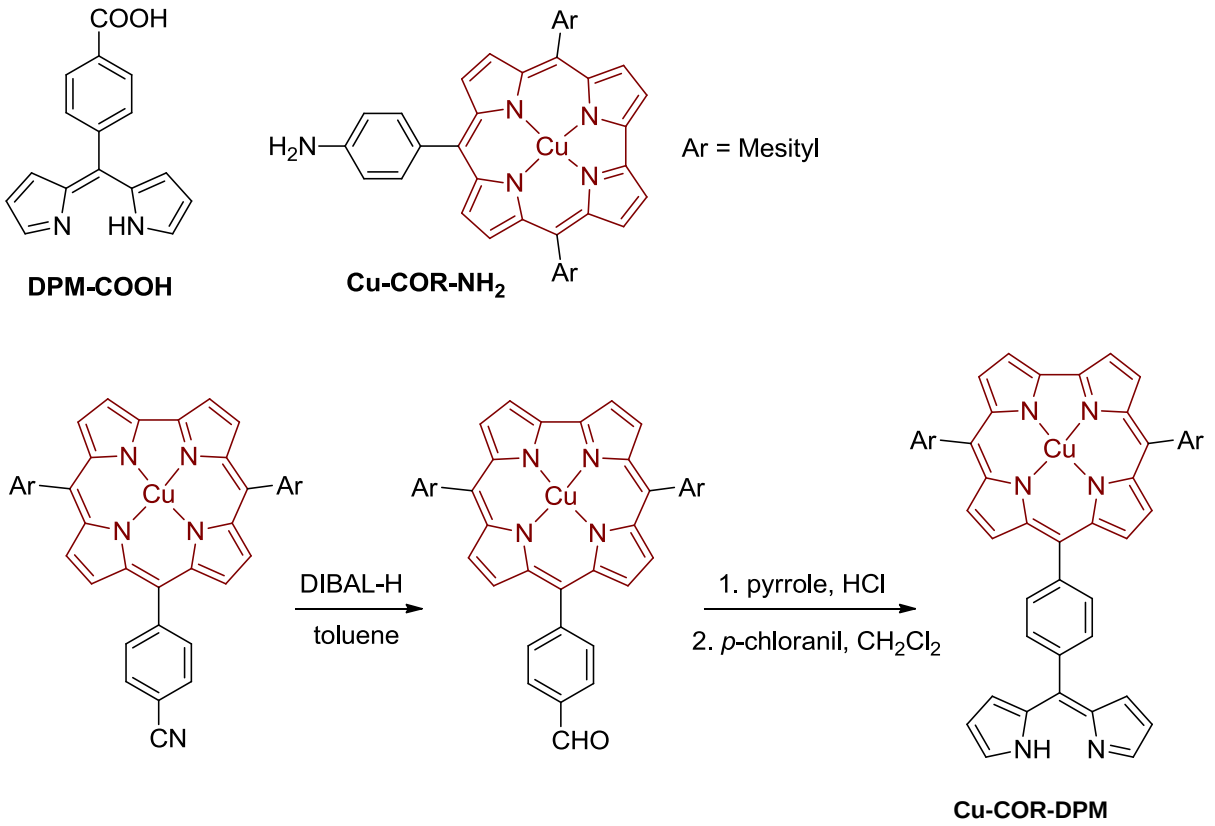

Scheme 1. Overview of the oligopyrrole materials applied and synthetic route toward copper corrole-dipyrromethene conjugate Cu-COR-DPM.

3.1. Characterization of copper redox active SAMs by Cyclic voltammetry and Osteryoung square-wave voltammetry

The electrochemistry of (metallo)corroles in organic solvents is relatively well described [29-31,35,36]. Churchill *et al.*[31] assigned the oxidation potential of a *meso*-thienyl-substituted copper corrole (on a gold disc electrode in benzonitrile *vs.* Fc/Fc^+) at *ca.* 0.27 V to a corrole-centered oxidation, while the reduction at -0.57 V *vs.* Fc/Fc^+ was assigned to the metal center. However, there are not so many scientific data concerning the electrochemistry of dipyrromethenes in organic solvents [28] or in aqueous solutions [23]. The reduction of a Cu-dpym (dpym=3,3',5,5'-tetramethyl-4.4'-dicarboethoxy-dipyrromethene) in acetone, occurring at -290 mV *vs.* SCE, was reported by Metelski *et al.*[28].

In our previous article [23] we have presented redox active SAMs based on dipyrromethene – Cu(II) complex. The objective of that paper was an elaboration of Cu(II) surface complexation and exploring the charge transfer in the mono-redox active SAMs depending on the distance of redox sites from the electrode surface.

The main objective of the research presented is exploring the charge transfer in the redox – active SAMs incorporating two different redox sites: dipyrromethene–Cu(II) and corrole – Cu complexes, located within one molecule one over another. There are articles concerning multi- redox SAMs. But the redox sites are located “side by side”. To our knowledge, there is little scientific report

concerning redox SAM configuration similar to the system presented in our manuscript [2]. The charge transfer in mono- redox active sites SAMs Cu-DPM, Cu-COR as well as multi- redox active sites SAM Cu-DPM-Cu-COR (Scheme 2) have been characterized and compared.

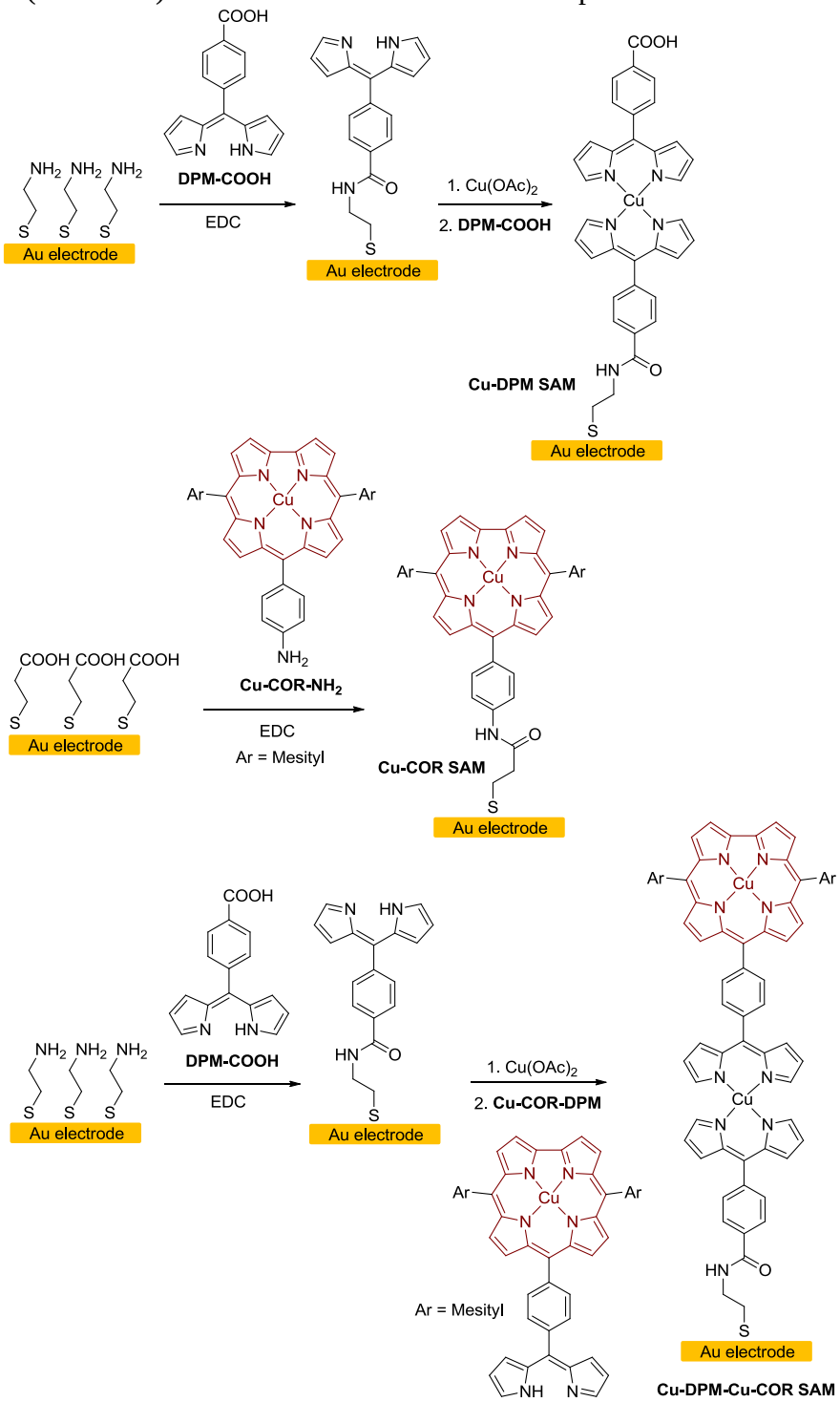

Scheme 2. Overview of the different gold electrode modification routes.

All SAMs were characterized by CV and OSWV performed in 0.1 M KCl. The CVs recorded at 100 mVs^{-1} for gold electrodes modified with a layer of Cu-DPM (Figure 1) showed a *quasi* reversible redox couple of anodic and cathodic peaks at ca. 266 ± 2 mV and 199 ± 10 mV,

respectively. On the other hand, the Cu-COR complex deposited on the gold electrode displayed its redox activity at a negative potential (Figure 1), with *quasi* reversible anodic and cathodic peaks recorded at -217 ± 10 mV and -282 ± 10 mV, respectively. The SAM consisting of both copper sites, the Cu-DPM-Cu-COR SAM, demonstrated two pairs of peaks, at positive (195 ± 14 mV and 146 ± 5 mV) and negative potential (-208 ± 2 mV, not so well-defined, and -357 ± 22 mV) (Figure 1). During CV measurements we did not observed Cu redox sites releasing from the film. The cyclic-voltammograms remained invariable when potential were cycled in the potential windows described in experimental section. Thus, we can conclude that the binding of Cu by dipyrromethene and corrole is strong enough to stay in the self-assembled monolayers. In addition, the CV experiments were finished at the potential which ensured the more stable oxidation state of Cu sites. The cyclic voltammetry of Cu(II)-DPM complexes have been performed in organic solvent such as acetone or dichloromethane [28]. It has been confirmed that electrochemical reduction of Cu(II) –dipyrromethene complex did not undergo ligand loss and ligand was not irreversibly altered in this process. These facts suggest rapid electron transfer to and from Cu centre. The electrochemistry of Cu – corrole complexes have been also performed in the organic solvents. In general, results showed that the reduction is metal centered, while oxidation is corrole centered. The demetalation of corrole complexes is very difficult and demands harsh acidic conditions. The difficulty of corrole demetalation could be attributed to: (i) smaller core and shorter nitrogen – metal bonds in comparison to porphyrines, (ii) higher valency of metal ion; (iii) better donor properties, higher acidity than porphyrines. Thus, we can state that during the electrochemical experiments both complexes self- assembled on the electrode surface did not undergo demetalation or decomposition.

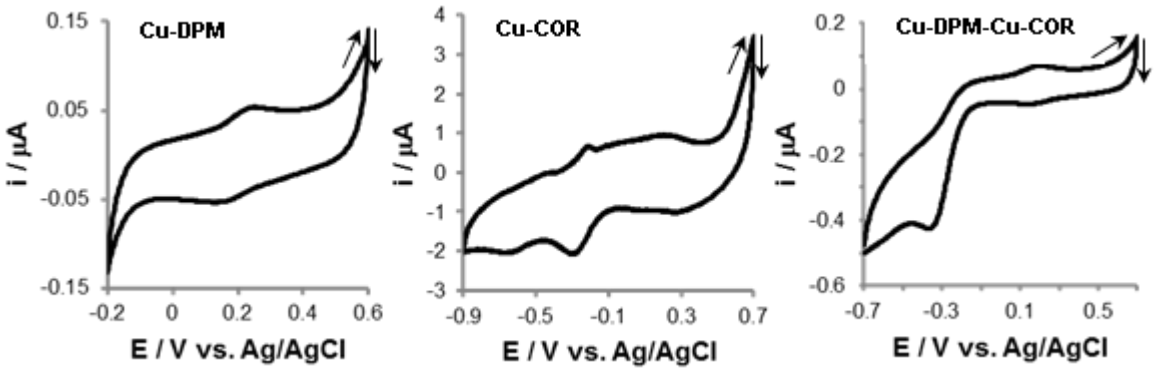

Figure 1. Cyclic voltammograms obtained for gold electrode modified by: Cu-DPM, Cu-COR and Cu-DPM-Cu-COR. Scan rate 100 mVs^{-1}, reference electrode Ag/AgCl, counter electrode Pt.

The presence of the Cu-COR in the SAM shifted the anodic and cathodic peaks of the copper dipyrromethene part in the negative direction, by -71 mV and -53 mV, respectively. The shift of the cathodic peak of the Cu-COR in the mixed SAM was similar, -75 mV. On the other hand, the anodic peak of the Cu-COR was very poorly defined in the mixed SAM, and its position remained almost unchanged.

Based on these data we can conclude that the process of oxidation of the copper dipyrromethene sites is facilitated by the presence of the copper corrole in the mixed SAM. The possible reason for this phenomenon might be the increase of electron density at the DPM due to the vicinity of the Cu-COR sites. The reduction processes of both types of Cu sites are hindered in the multi-Cu SAM in comparison to the mono-Cu SAM. This influence was a little stronger for the Cu-COR SAM (-75 mV) than for the Cu-DPM SAM (-53 mV).

The mutual influence of both types of Cu sites deposited on the gold electrode surface was illustrated also by other electrochemical parameters. A half-wave potential ($E_{1/2}$) shift of both redox centers in the multi-Cu SAM to the negative potential direction was recorded. The $\Delta E_{1/2}$ for the Cu-DPM SAM (-62 mV) was larger than the $\Delta E_{1/2}$ observed for the Cu-COR SAM (-33 mV) (Table 1).

Table 1. Electrochemical parameters of different type of SAMs: Cu-DPM, Cu-COR and Cu-DPM-Cu-COR obtained from CV and OSWV in 0.1 M KCl (n=5).ΔE_p is the peak to peak separation, $E_{1/2}$ is the formal potential, E_{fwhm} is the full width at half-maximum, E_{max} is the value of max peak potential in OSWV, I_{pa}/I_{pc} is the ratio of the anodic to the cathodic peak current.

Type of modification	ΔE_p [mV] (CV)	$E_{1/2}$ [mV] (CV)	E_{fwhm} [mV] (CV)	E_{max} [mV] (OSWV)	I_{pa}/I_{pc}
Cu-DPM	67 ± 5	233 ± 6	135 ± 5	218 ± 10	1.1
Cu-COR	65 ± 10	- 250 ± 10	134 ± 5	- 187 ± 3	0.3
Cu-DPM− Cu-COR	49 ± 10 149 ± 12	171 ± 10 - 283 ± 12	128 ± 22 153 ± 15	188 ± 8 - 260 ± 18	1.3 0.1

The values of the peak to peak separation (ΔE_p) and the full width at half-maximum (E_{fwhm}) for all SAMs studied deviated from the values characteristic for an ideal reversible electrochemical system, when oxidized and reduced species were strongly adsorbed to the electrode (Table 1). In the ideal situation, ΔE_p is equal to 0 at low scan rates, whereas E_{fwhm} should be 90.6 mV (at 25 °C) [37,38]. The deviation from these values indicated the disorder within the SAMs and the lack of homogeneity of the redox centers on the surface of the gold electrodes due to electrostatic interactions (attractive or repulsive) among the redox sites, as was reported by others [39,40]. However, the presence of both copper sites improved the reversibility of the Cu-DPM site. The ΔE_p value decreased from 67 to 49

mV. The opposite phenomenon was observed for the Cu-COR present in the mixed SAM. The ΔE_p value increased from 65 to 149 mV (Table 1). The same tendency was observed for the full width at half-maximum (E_{fwhm}) values. This parameter was comparable for the Cu-DPM and Cu-COR SAMs (Table 1). In the mixed SAM, a slightly better E_{fwhm} was observed for Cu-DPM, and at the same time a slightly worse E_{fwhm} for Cu-COR (Table 1).

The reversibility of the redox system might be estimated by the ratio of the anodic to the cathodic peak current (I_{pa}/I_{pc}). The values recorded for Cu-DPM in the mono- and multi-Cu-SAMs are close to ~1.1–1.3, indicating good reversibility [37,38]. The reversibility of Cu-COR, both in the mono- and multi-Cu SAMs, was definitely worse. The ratio I_{pa}/I_{pc} was in the range ~ 0.1–0.3.

The mono- and multi-Cu SAMs were also characterized using Osteryoung square-wave voltammetry [41,42], a more sensitive and more suitable technique to analyze systems displaying large capacitive currents. The peak currents for the Cu-DPM and Cu-COR SAMs were well-defined at 218 ± 10 mV and -187 ± 3 mV, respectively. The mixed Cu-DPM-Cu-COR SAM induced two well-defined and separated peaks, at a positive potential of 188 ± 8 mV and a negative potential of -260 ± 18 mV (Figure 2). Both peaks obtained for the multi-Cu SAM were negatively shifted in comparison to the mono-Cu SAMs. The shift of the potential recorded at maximum redox current was larger for Cu-COR (-73 mV) than for Cu-DPM (-30 mV) (Table 1). With using this technique, two well separated peaks connected with two different redox sites were observed, and we were able to record the difference between charge transfer in mono-redox active sites SAMs and multi-redox active SAM.

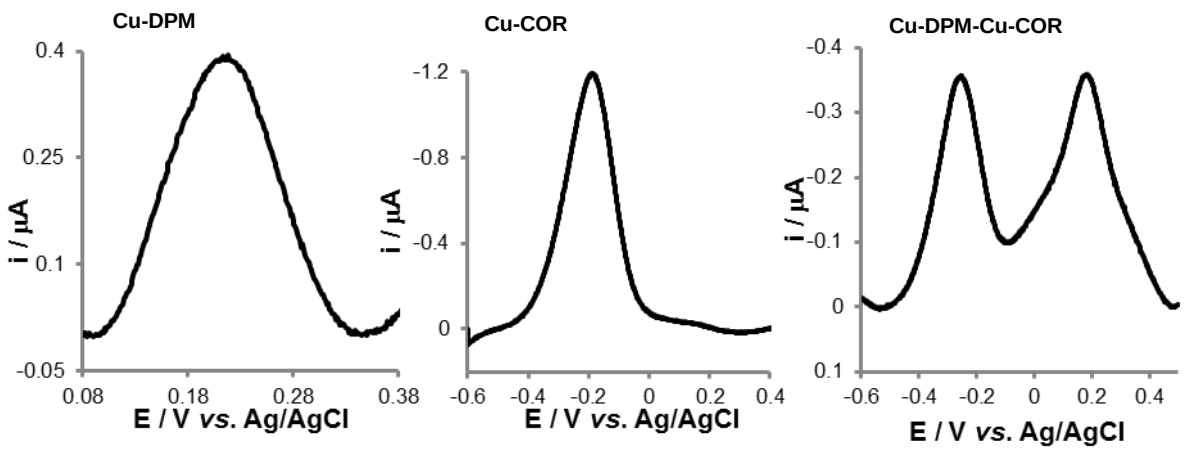

Figure 2. Osteryoung square wave voltammograms obtained for gold electrode modified by: Cu-DPM, Cu-COR, Cu-DPM-Cu-COR in 0.1 M KCl solution, step potential: 10 mV, square-wave frequency: 25 Hz, and square-wave amplitude 25 mV.

One can also observe differences in current intensity of Cu-DPM SAM and Cu-COR SAM (Figures 1 and 2). In our opinion, there are two main reasons of this phenomenon: the differences in the structure of these two Cu complexes and the different way of their immobilization on the Au surface. The several different coordination types are known for metallo-corroles, but the most common is square planar. The corrole–Cu complexes exhibit interesting electronic configuration with hybrid Cu(III) and Cu(II) π – cation character, with majority Cu(III) character. They tend to be strongly

saddled [21]. The electrochemical HOMO-LUMO gap for Cu corrolates is quite low, lending future support to the notion that oxidation occurs on corrole ring, while the reduction occurs at the copper center [43]. The structure of Cu-DPM complex is close to tetrahedral [28]. Such Cu(II) complex is interesting in that the dipyrromethene ligands provide a porphyrin – like environment, but with tetrahedral rather than square-planar disposition of four N donor atoms about Cu. The tetrahedral geometry ensures the some degree of flexibility, which may lower electron transfer rates relative to those of encapsulating ligand systems by increasing Frank-Condon barrier.

The Cu-DPM and Cu-corrole are attached to the electrode surface via peptide bonds. But these bonds are oriented in the different way toward the electrode surface: -NH-CO- and –CO-NH-, respectively. This could also influence on the rate of electron transfer.

The above described parameters could explain the difference in the intensity of reduction/oxidation copper current of all SAMs studied. These differences are higher when cyclic voltammetry was applied. This is mainly due to high capacity current (Figure 1). When OSWV was used, the peaks become better defined. The differences in the intensity of reduction/oxidation copper current between all SAMs studied become smaller, but the sequence remained the same: Cu-COR > Cu-DPM $\geq$ Cu-DPM-Cu-COR.

Based on the results obtained with CV and OSWV, we can conclude that the reduction of the different copper sites assembled together in the mixed SAM is hindered, and more for Cu-COR than for Cu-DPM. Apart from the mutual interactions between the two Cu sites, the larger distance of the Cu-COR sites from the gold electrode surface might be a reason for its hindered redox reaction. Moreover, the environment around both single-Cu complexes is changed when they are incorporated into the mixed Cu-DPM-Cu-COR SAM. Thus, the accessibility of the ions present in the supporting electrolyte to the copper redox centers is changed and the kinetics of the redox reactions are altered [44].

3.2. Electrochemical impedance spectroscopy in the presence of $[Fe(CN)_6]^{3-}/[Fe(CN)_6]^{4-}$

Over the last decade, electrochemical impedance spectroscopy, being an extraordinarily versatile, sensitive, and non-invasive technique, has become one of the most popular analytical tools widely applicable for electrochemical kinetics studies at electrode-media interfaces [45]. The method is very frequently used for the characterization of gold electrodes modified with SAMs containing redox-active molecules [33,34,37,46].

To explore the electron transport kinetics occurring at the electrodes modified with the Cu-DPM, Cu-COR and Cu-DPM-Cu-COR SAMs, electrochemical impedance spectroscopy was performed in the presence of 2 mM $[Fe(CN)_6]^{3-}/[Fe(CN)_6]^{4-}$ at the formal potential of 170 mV. The applied potential, characteristic for $[Fe(CN)_6]^{3-}/[Fe(CN)_6]^{4-}$ is in range of the oxidation processes of copper complexed with dipyrromethene, both in single and multi –Cu-SAM. However, $[Fe(CN)_6]^{3-}/[Fe(CN)_6]^{4-}$ is the most popular external redox probe suitable for impedance measurements, because both its forms are stable. In addition, similar conditions have been already reported for impedance study of redox active monolayers incorporated ferrocene or cobalt(II)tetra-aminophthalocyanine which

displayed oxidation process in the similar range as $[Fe(CN)_6]^{3-}/[Fe(CN)_6]^{4-}$ used as the external redox probe [34,47].

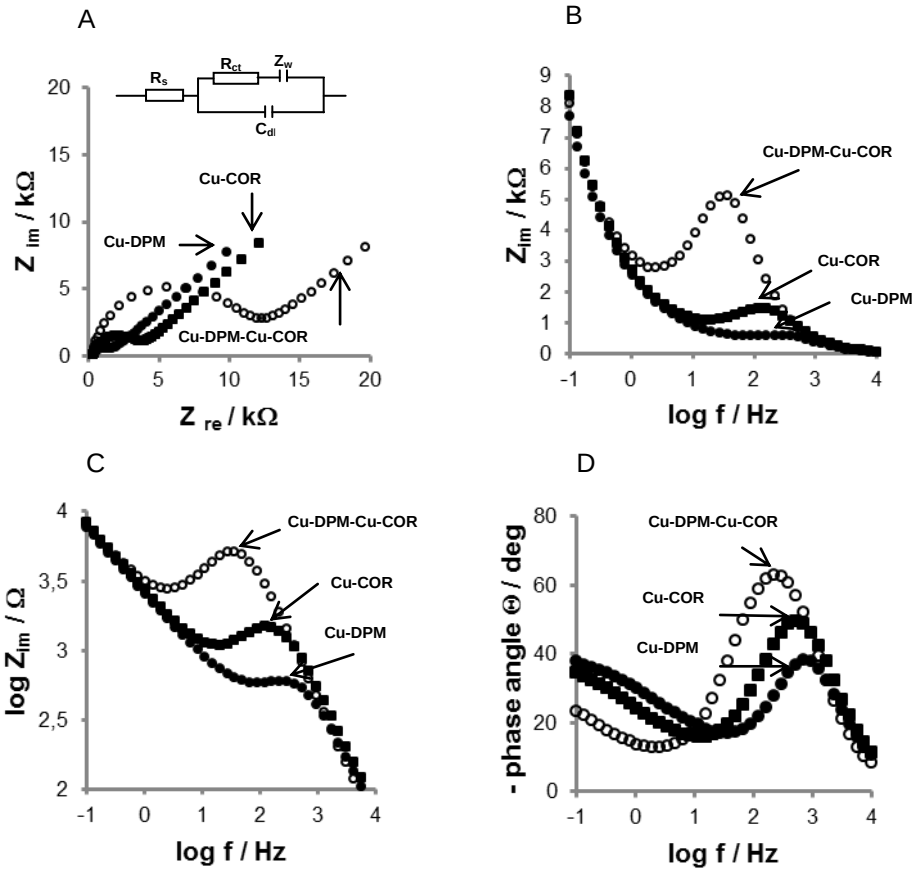

Figure 3. (a) Electrochemical impedance spectra obtained for gold electrodes modified by Cu-DPM (•),Cu-COR (■) and Cu-DPM-Cu-COR (o) in the presence of 2 mM $Fe[(CN)_6]^{3-}/Fe[(CN)_6]^{4-}$. Bias potential of 170 mV. The frequency ranges from 0.1 to 10 kHz. **(b)** Imaginary part (Z_{im}) of the impedance as a function of log frequency for gold electrodes modified by Cu-DPM (•),Cu-COR (■) and Cu-DPM-Cu-COR (o) in 2 mM $Fe[(CN)_6]^{3-}/Fe[(CN)_6]^{4-}$. **(c)** Logarithm of Z_{im} as a function of log frequency for gold electrodes modified by Cu-DPM (•),Cu-COR (■) and Cu-DPM-Cu-COR (o) in 2 mM $Fe[(CN)_6]^{3-}/Fe[(CN)_6]^{4-}$. **(d)** Bode plots (phase angle Θ *vs*. log f) for gold electrodes modified by Cu-DPM (•),Cu-COR (■) and Cu-DPM-Cu-COR (o) in 2 mM $Fe[(CN)_6]^{3-}/Fe[(CN)_6]^{4-}$.

The Nyquist plots (imaginary impedance component [Z_{im}] plotted against the real impedance component [Z_{re}] at each excitation frequency) for all SAMs studied are presented in Figure 3A. These plots exhibited a characteristic course with semicircles at high frequencies observed for the electron transfer limited process and a straight line at low frequencies, which represents a diffusion limited process. The semicircle diameters in the Nyquist plots were different for each particular SAM and are connected with the different values of the charge transfer resistance, which are related to the activation energy and the distance between the species and the electrode where the charge transfer may occur

[45]. The spectra obtained under open circuit conditions were fitted according to the following equivalent circuit, $R_s(C_{dl}[R_{ct}Z_w])$ [33,34], in which R_s is the electrolyte solution resistance, R_{ct} the charge-transfer resistance, C_{dl} the true double layer capacitance, and Z_w the Warburg impedance. The best fitting parameters were obtained when C_{dl} was treated as a constant phase element CPE_{dl}, while Z_w as CPE_W.

The R_{ct} values determined for both mono-Cu site SAMs were very similar, in the range of 1 kΩ (Figure 3A, Table 2). After incorporation into the Cu-DPM-Cu-COR SAM, R_{ct} increased *ca.* 7 times to 7.72 ± 2.20 kΩ. Based on the R_{ct} values obtained from the fitted Nyquist plots for each SAM, the apparent standard rate constant (k_{app}) was calculated using the equation (1) [48,49]:

$$k_{app} = \frac{RT}{n^2F^2Ac_0R_{ct}} \quad (1)$$

where A is the electrode area, c_0 the concentration of the redox probe, and R_{ct} the charge-transfer resistance, F is the Faraday constant, n is the number of electrons exchanged, R gas constant, T absolute temperature. The k_{app} values for both mono-Cu site SAMs were similar, and in the range of 7–8 x 10^{-3} cms^{-1}. The incorporation into the Cu-DPM-Cu-COR SAM results in a decrease of the k_{app} values to the ~1 x 10^{-3} cms^{-1}. The possible reason for the lower permeability toward $[Fe(CN)_6]^{3-}$/$[Fe(CN)_6]^{4-}$ might be the higher SAM thickness.

Table 2. Electrochemical impedance spectroscopy parameters obtained in 0.1 M KCl in the presence of $[Fe(CN)]_6^{3-}$/$[Fe(CN)_6]^{4-}$ for different type of SAMs: Cu-DPM, Cu-COR and Cu-DPM-Cu-COR (n=5). R_s is the electrolyte solution resistance, CPE_{dl} *is* C_{dl} (double layer capacitance) treated as a constant phase element (CPE), R_{ct} is the electron transfer resistance, CPE_W is Z_W (Warburg impedance) treated as CPE, k_{app} is the apparent standard rate constant.

SAM	R_s [Ω]	CPE_{dl} [μF]	R_{ct} [kΩ]	CPE_W [μF]	k_{app} [cms^{-1}]
Cu-DPM	244±18	0.53±0.06	1.15±0.34	0.112±0.002	7.37 x 10^{-3}
Cu-COR	254±1	0.52±0.05	1.22±0.28	0.111±0.004	6.94 x 10^{-3}
Cu-DPM–Cu-COR	269±18	0.50±0.07	7.72±2.2	0.101±0.007	1.10 x10^{-3}

In the case of electrochemical impedance spectroscopy, the data can be presented in modulus, dielectric and impedance domains. The information obtained is independent of the chosen representation method. Therefore, we have decided to keep all relationships as presenting in Figure 3.

The plots log Z_{im} vs. log *f* provides information about "distributed processes" where capacitance in the circuit is not ideal and the Nyquist plots shows depressed or deformed semicircular feature. It results in a straight line with a constant slope within the frequency range Δ log *f* above the critical relaxation frequency f_c. The slope value was estimated as [45]:

$$\alpha = \frac{arctan\Delta Zim}{\Delta log f} \quad (2)$$

and the value of the α-parameter could indicative a degree of nonideality [45]. The -45º angle corresponds to α = 1, indicating that the imaginary impedance component Z_{im} is described by an ideal capacitor. The deviation from α ≠ 1 indicates a nonideal pseudo capacitive behavior. From the plots of Z_{im} vs. log *f* in Figure 3B we have determined critical relaxation frequency f_c. They are as follow: $f_{c,\ Cu\text{-}DPM}$ = 289.4 Hz, $f_{c,\ Cu\text{-}COR}$ = 119.4 Hz and $f_{c,\ Cu\text{-}DPM\text{-}Cu\text{-}COR}$ = 36.7 Hz. For SAM incorporated both Cu sites the f_c value was the lowest. From the slopes of relationships log Z_{im} vs. log *f* in Figure 3C we have determined α parameter values for all SAMs studied. The obtained values were as follow: $\alpha_{Cu\text{-}DPM}$ = 0.73 in the frequency range from log *f* = 4.0 to log *f* = 2.7; $\alpha_{Cu\text{-}COR}$ = 0.79 in the frequency range from log *f* = 4.0 to log *f* = 2.3; $\alpha_{Cu\text{-}DPM\text{-}Cu\text{-}COR}$ = 0.90 in the frequency range from log *f* = 4.0 to log *f* = 1.9. These values are lower than 1 and indicated the *pseudo* capacitive behavior of all SAMs studied. The highest α value, nearest to one, was recorded for Cu-DPM-Cu-COR SAM, where two different Cu sites are incorporated.

From the plots of the phase angle *Θ vs*. log *f* (Figure 3D), one can observe that the frequencies of the maximum phase angle *Θ* observed for the Cu-DPM SAM (log *f* = 3.0) and the Cu-COR SAM (log *f* = 2.9) were very similar. This indicates a similar electrochemical reaction rate. When both Cu sites were incorporated in the mixed SAM, the maximum phase angle *Θ* was observed at lower frequency (log *f* = 2.3). This means that the electrochemical reaction rate for the multi-Cu SAM was lower, as *f* is related to the time constants of an electrochemical reaction [34].

The maximum values of the phase angle also allowed estimating the ion permeability of the SAMs. When SAMs behave like ideal capacitors, the phase angle is equal or greater than 90°. Values lower than 90° indicate that the SAMs are permeable to ions from solution [34,47].

The maximum values of the phase angle recorded for the SAMs studied here were as follows: *ca*. 38° for the Cu-DPM SAM, *ca*. 49° for the Cu-COR SAM, and *ca*. 63° for the Cu-DPM-Cu-COR SAM (Figure 3C). The highest permeability of Cu-DPM SAM to ions from solution might be caused by the presence of COOH groups, which make this particular SAM the most hydrophilic. Another SAMs do not posses any hydrophilic groups. The incorporation of Cu-COR sites to Cu-DPM SAM decreased the permeability to ions from solution. For this SAM the phase contact angle is the highest (63°).

3.3. Electrochemical impedance spectroscopy in the absence of an external redox probe

To probe the heterogeneous electron transfer kinetics at the gold electrodes modified with the mono- and multi-Cu SAMs, electrochemical impedance spectroscopy was performed in electrolyte solution in the absence of an external redox probe [33,34,49-51]. The Nyquist plots of the gold electrodes modified with all SAMs studied were recorded at the formal potential of the redox-active

molecules deposited on the electrode surfaces (Figure 4A) [33,34]. The experimental data were fitted to the equivalent circuit $R_s(C_{dl}[R_{ct}C_{ad}])$. The best fitting was obtained when the double layer capacitance C_{dl} and the adsorption pseudo-capacitance C_{ad} were replaced by constant phase elements, CPE_{dl} and CPE_{ad}, respectively. Based on the results obtained, the electron transfer rate constants k_{et} for each SAM were calculated using the equation (2) [33,34,50,52]

$$k_{et} = \frac{1}{(2R_{ct}C_{ad})} \qquad (3)$$

The highest value of R_{ct} was obtained for the Cu-DPM SAM. The R_{ct} of the Cu-COR SAM was *ca*. 7 times lower (Table 3). When both complexes were incorporated into the mixed SAM, the R_{ct} values recorded at the potentials characteristic for the Cu-DPM SAM (184 mV) and the Cu-COR SAM (-256 mV) were lower than the values recorded for the mono-Cu SAMs (Table 3). The CPE_{ad} values associated with the capacitance of the redox-active layer recorded for the Cu-DPM and Cu-COR sites were in the range of 0.40–0.77 μF and 8.24–24.2 μF, respectively. The values of R_{ct} as well as CPE_{ad} have an influence on the electron transfer rate constant k_{et}. The highest k_{et} value was obtained for the multi-Cu SAM recorded at a positive potential (184 mV) characteristic for the Cu-DPM sites (Table 3). The lowest k_{et} values were obtained for the Cu-COR SAM and mixed SAM measured at negative potential (-256 mV).

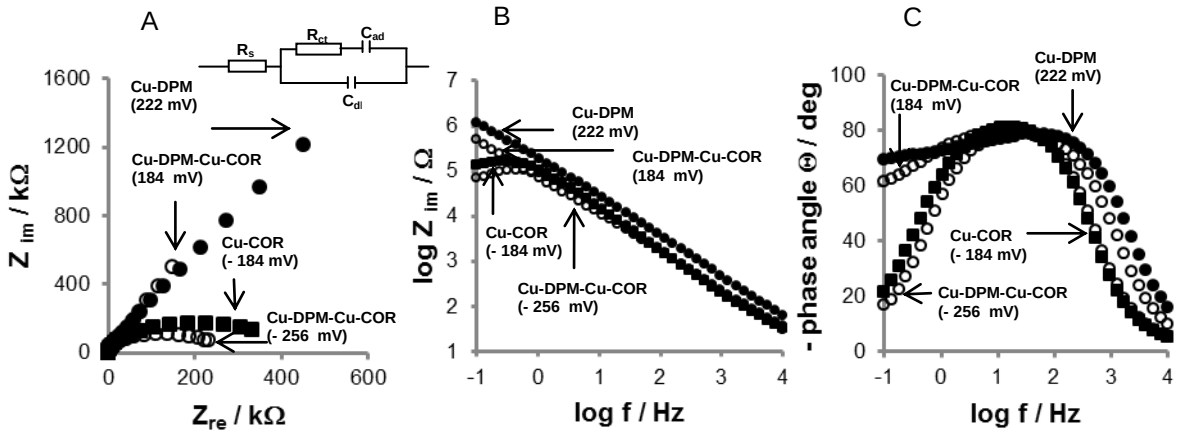

Figure 4. (a) Electrochemical impedance spectra obtained for gold electrodes modified by Cu-DPM (•), Cu-COR (■) and Cu-DPM-Cu-COR (o) at their approximate formal potential + 222 mV, - 184 mV, - 256 mV and + 184 mV, respectively. The frequency ranges from 0.1 to 10 kHz. **(b)** Logarithm of Z_{im} as a function of log frequency for gold electrodes modified by Cu-DPM (•),Cu-COR (■) and Cu-DPM-Cu-COR (o). **(c)** Bode plots (phase angle Θ *vs*. log f) for gold electrodes modified by Cu-DPM (•), Cu-COR (■) and Cu-DPM-Cu-COR (o).

When EIS measurements are performed in the absence of an external redox probe, the redox processes of the surface confined copper sites are explored. The linear relationships in the log Z_{im} *vs*. log *f* plots were observed in the range of log *f* = 4.0 to log *f* = -1.0 for SAMs: Cu-DPM and Cu-DPM-Cu-COR measured at potential characteristic for Cu-DPM (Figure 4B). For the other SAMs: Cu-COR

and Cu-DPM-Cu-COR measured at potential characteristic for Cu-COR, the linear relationships were observed in range: log f = 4.0 to log f = -0.23. The slope values of $\alpha_{Cu\text{-}DPM}$ = 0.87, $\alpha_{Cu\text{-}COR}$ = 0.90, $\alpha_{Cu\text{-}DPM\text{-}Cu\text{-}COR}$ = 0.83 (measured at potential characteristic for Cu-DPM) and $\alpha_{Cu\text{-}DPM\text{-}Cu\text{-}COR}$ = 0.89 (measured at potential characteristic for Cu-COR) were in the same range and confirmed the *pseudo* capacitive behavior of all SAMs. The *pseudo* capacitive behavior was confirmed by the maxima of the peaks of the phase angle (-ϕ) vs. log f plots, that were in the range of 77–80° (Figure 4C). These values, greater than 45°, are also characteristic for reversible process, in which reversible charge transfer to a surface layer mimics the reversible charging and discharging of a capacitor [48].

Table 3. Electrochemical impedance spectroscopy parameters obtained at the formal potential of redox active complexes in 0.1 M KCl for different type of SAMs: Cu-DPM, Cu-COR and Cu-DPM-Cu-COR (n=3-5). R_s is the electrolyte solution resistance, CPE_{dl} is C_{dl} (double layer capacitance) treated as a constant phase element (CPE), R_{ct} is the charge-transfer resistance, CPE_{ad} is C_{ad} (the adsorption pseudo-capacitance) treated as CPE, k_{et} is electron transfer rate constants.

SAM	formal potential	R_s [Ω]	CPE_{dl} [μF]	R_{ct} [kΩ]	CPE_{ad} [μF]	k_{et} [s^{-1}]
Cu-DPM	+ 222 mV	217±3	0.66±0.12	1182±112	0.40±0.16	1.06
Cu-COR	- 184 mV	259±7	2.89±0.02	152.8±9.0	24.2±3.6	0.14
Cu-DPM−Cu-COR	+ 184 mV	263±5	0.71±0.08	413.3±143	0.77±0.18	1.57
Cu-DPM−Cu-COR	- 256 mV	265±5	0.76±0.03	118.9±29.3	8.24±2.19	0.51

4. CONCLUSIONS

In this work, the electrochemistry of a dipyrromethene-copper complex, a copper corrole and a novel copper dipyrromethene-copper corrole conjugate self-assembled on the surface of gold electrodes was analyzed in aqueous solutions. The Osteryoung square-wave voltammetry (OSWV) reduction/oxidation peak of copper complexed with dipyrromethene ligands occurred at a positive potential (218 ± 10 mV), whereas this occurred at a negative potential

(- 187 ± 3 mV) for the copper corrole derivative. When both complexes were immobilized together in a mixed SAM, two well-defined and separated peaks were observed in OSWV, at the potential of 188 ± 10 mV and -260 ± 18 mV. The negative shift of both of them indicated that the reduction processes are hindered in the multi-Cu site SAM.

The work presented opens the way for creation of new multi redox sites monolayer which offer the possibilities of tuning their electrochemical properties.

ACKNOWLEDGEMENTS
This work was supported by the EU grant COST CM1005 "Supramolecular Chemistry in Water", 679/N-BELGIA/2010/0 and the Institute of Animal Reproduction and Food Research of the Polish Academy of Sciences, Olsztyn, Poland. We also thank the F.W.O.-Vlaanderen and the KU Leuven for financial support. T.H.N. further acknowledges the IWT (Institute for the Promotion of Innovation through Science and Technology in Flanders) and the Alexander von Humboldt Foundation for a doctoral and postdoctoral fellowship, respectively.

References

1. M. Haga, K. Kobayashi, K. Terada, *Coord. Chem. Rev.,* 251 (2007) 2688.
2. H. Nishihara, K. Kanaizuka, Y. Nishimori, Y. Yamanoi, *Coord. Chem. Rev.,* 251 (2007) 2674.
3. S. Liatard, J. Chauvin, F. Balestro, D. Jouvenot, F. Loiseau, A. Deronzier, *Langmuir,* 28 (2012) 10916.
4. Ch. H.-H. Traulsen, E. Darlatt, S. Richter, J. Poppenberg, S. Hoof, W. E. S. Unger, Ch. A. Schalley, *Langmuir,* 28 (2012) 10755.
5. B. Viguier, K. Zór, E. Kasotakis, A. Mitraki, C. H. Clausen, W. E. Svendsen, J. Castillo-León, *ACS Appl. Mater. Interfaces,* 3 (2011) 1594.
6. J. Liu, M. Chen, D.-J. Qian, *Langmuir,* 28 (2012) 9496.
7. M. Maskus, H. D. Abruna, *Langmuir,* 12 (1996) 4455.
8. M. Utsuno, F. Toshimitsu, S. Kume, H. Nishihara, *Macromol. Symp.* 270 (2008) 153.
9. N. Tuccitto, I. Delfanti, V. Torrisi, F. Scandola, C. Chiorboli, V. Stepanenko, F. Wurthner, A. Liciardello, *Phys. Chem. Chem. Phys.,* 11 (2009) 4033.
10. A. Winter, S. Hoeppener, G. R. Newkome, U. S. Schubert, *Adv. Mater.,* 23 (2011) 3484.
11. W. Maes, W. Dehaen, *Pol. J. Chem.,* 82 (2008) 1145.
12. W. Van Rossom, O. Kundrát, T. H. Ngo, P. Lhoták, W. Dehaen, W. Maes, *Tetrahedron Lett.,* 51 (2010) 2423.
13. W. Maes, W. Dehaen, *Synlett,* (2003) 79.
14. W. Maes, T. H. Ngo, J. Vanderhaeghen, W. Dehaen, *Org. Lett,*. 9 (2007) 3165.
15. T. H. Ngo, F. Nastasi, F. Puntoriero, S. Campagna, W. Dehaen, W. J. Maes, *Org. Chem.,* 75 (2010) 2127.
16. T. H. Ngo, F. Puntoriero, F. Nastasi, K. Robeyns, L. Van Meervelt, S. Campagna, W. Dehaen, W. Maes, *Chem. Eur. J.,* 16 (2010) 5691.
17. T. H. Ngo, W. Van Rossom, W. Dehaen, W. Maes, *Org. Biomol. Chem.,* 7 (2009) 439.
18. F. Nastasi, S. Campagna, T. H. Ngo, W. Dehaen, W. Maes, M. Kruk, *Photoch. Photobio. Sci.,* 10 (2011) 143.
19. T. Rohand, E. Dolusic, T. H. Ngo, W. Maes, W. Dehaen, *ARKIVOC,* 10 (2007) 307.
20. W. Nulens, I. Grabowska, T. H. Ngo, W. Maes, W. Dehaen, H. Radecka, J. Radecki, *J. Incl. Phenom. Macro.,* 71 (2011) 499.
21. J. H. Palmer, *Struct. Bond,* 142 (2012) 49.

22. S. Viswanathan, Y. Z. Voloshin, H. Radecka, J. Radecki, *Electrochim. Acta*, 54 (2009) 5431.
23. I. Szymanska, M. Stobiecka, Cz. Orlewska, T. Rohand, D. Janssen, W. Dehaen, H. Radecka, *Langmuir*, 24 (2008) 11239.
24. I. Szymanska, Cz. Orlewska, D. Janssen, W. Dehaen, H. Radecka, *Electrochim. Acta*, 53 (2008) 7932.
25. Ch. Bruckner, V. Karunaratne, S. J. Rettig, D. Dolphin, *Can. J. Chemistry*, 74 (1996) 2182.
26. K. Heinze, A. Reinhart, *Inorg. Chem.*, 45 (2006) 2695.
27. S. R. Halper, M. Malachowski, H. M. Delaney, S. M. Cohen, *Inorg. Chem.*, 43 (2004) 1242.
28. P. D. Metelski, A. S. Hinman, H. D. Takagi, T. W. Swaddle, *Can. J. Chemistry*, 73 (1995) 61.
29. A. Ghosh, E. J. Steene, *Inorg. Biochem.*, 91 (2002) 423.
30. W. D. Kerber, D. P. Goldberg, *J. Inorg. Biochem.*, 100 (2006) 838.
31. N. Maiti, J. Lee, S. J. Kwon, J. Kwak, Y. Do, D. G. Churchill, *Polyhedron*, 25 (2006) 1519.
32. F. Isaacs, W. Dehaen, W. Maes, T. H. Ngo, D. Ruiz-Leon, F. Herrera, R. Arce, C. Arevalo, M. Aguirre, J. *Int. J. Electrochem. Sci.*, 8 (2013) 3406.
33. E. Katz, O. Lioubashevsky, I. Willner, *J. Am. Chem. Soc.*, 126 (2004) 15520.
34. D. Nkosi, J. Pillay, K. I. Ozoemena, K. Nouneh, M. Oyama, *Phys. Chem. Chem. Phys.*, 12 (2010) 604.
35. K. M. Kadish, V. A. Adamian, E. Van Caemelbecke, E. Gueletii, S. Will, Ch. Erben, E. Vogel, *J. Am. Chem. Soc.*, 120 (1998) 11986.
36. K.M. Kadish, W. Koh, P. Tagliatesta, D. Sazou, R. Paolesse, S. Licoccia, T. Boschi, *Inorg. Chem.*, 31 (1992) 2305.
37. A. L. Eckermann, D. J. Feld, J. A. Shaw, T. J. Meade, *Coord. Chem. Rev.*, 254 (2010) 1769.
38. H. O. Finklea, In *Electroanalytical Chemistry*; A. J. Bard, I. Rubinstein Eds.; Marcel Dekker Inc.: New York, Vol. 19, (1996).
39. A. L. Eckerman, J. A. Shaw, T. J. Meade, *Langmuir*, 26 (2010) 2904.
40. Ch. E. D. Chidsey, C. R. Bertozzi, T. M. Putvinsky, A. M. Mujsce, *J. Am. Chem. Soc.*, 112 (1990) 4301.
41. J. Osteryoung, *Acc. Chem. Res.*, 26 (1993) 77.
42. J. G. Osteryoung, R. A. Osteryoung, *Anal. Chem.*, 57 (1985) 101A.
43. A. Gosh, T. Wondimagegn, A.B.J. Parusel, *J. Am. Chem. Soc.*, 122 (2000) 5100.
44. S. E. Creager, G. K. Rowe, *J. Electroanal. Chem.*, 420 (1997) 291.
45. V. F. Lvovich, *In Impedance Spectroscopy: Applications to Electrochemical and Dielectric Phenomena*, John Wiley & Sons, Inc., (2012).
46. T. M. Nahir, E. F. Bowden, *Langmuir*, 18 (2002) 5283.
47. K. I. Ozoemena, T. Nyokong, D. Nkosi, I. Chambrier, M. J. Cook, *Electrochim. Acta*, 52 (2007) 4132.
48. A. J. Bard, L. R. Faulkner *In Electrochemical Methods – Fundamentals and Applications*, Second Edition, John Wiley & Sons, Inc., (2001).
49. F. Cecchet, M. Marcacio, M. Margotti, F. Paolucci, S. Rapino, P. Rudolf, *J. Phys. Chem. B*, 110 (2006) 2241.
50. T. M. Nahir, E. F. Bowden, *J. Electroanal. Chem.*, 410 (1996) 9.
51. E. J. Laviron, *J. Electroanal. Chem.*, 105 (1979) 35.
52. S. E. Creager, T. T. Wooster, *Anal. Chem.*, 70 (1998) 4257.

© 2014 by ESG (www.electrochemsci.org)